Quantum Electronics **48** (4) 306–312 (2018)

https://doi.org/10.1070/QEL16670

Femtosecond pulse self-shortening in Kerr media: role of modulational instability in the spectrum formation

Ya.V. Grudtsyn, A.V. Koribut, L.D. Mikheev, V.A. Trofimov

Abstract. **The mechanism of femtosecond pulse self-shortening in thin optical materials with Kerr nonlinearity is investigated. The experimentally observed spectral-angular distribution of the radiation intensity on the exit surface of a 1-mm-thick fused silica sample is compared with the results of numerical simulation based on solving the nonlinear Schrödinger equation for an electromagnetic wave with a transverse perturbation on the axis. Qualitative agreement between the calculated and experimental results confirms the hypothesis about the transient regime of multiple filamentation as a mechanism of femtosecond pulse self-shortening.**

Keywords: *self-shortening, femtosecond pulses, multiple filamentation, modulational instability, nonlinear Schrödinger equation.*

1. Introduction

Currently, the search for new methods of shortening the duration of high-power optical femtosecond pulses is one of the most urgent lines of research in nonlinear optics. Pulses as short as few optical cycles are of interest for various fundamental and applied studies, including high time resolution spectroscopy [1] and generation of GW-level THz pulses [2], as well as attosecond pulses in the far UV and soft X-ray ranges [3]. Spectral narrowing during amplification hinders the formation of pulses shorter than 20–30 fs in systems operating at multiterawatt and petawatt power levels. Thus, an urgent problem is to search for nonlinear methods making it possible to reduce the pulse duration at the output of these systems.

To date, different methods have been used to shorten high-power pulses. They all are based on nonlinear mechanisms of spectral broadening. With regard to their implementation, they can be separated into two groups. The first includes methods based on post-compression (i.e., compensation for the spectral phase acquired as a result of nonlinear spectral broadening) using additional dispersion elements (see, for example, [4, 5]). The second-group methods are based on self-compression. Here, the interaction of a pulse with matter leads to the formation of a transform-limited pulse; therefore, phase compensation is not required in this case. These methods were considered in the studies devoted to the reduction of pulse duration under filamentation in gas (see, for example, [6–8]), the compression of pulses in the soliton regime in the anomalous dispersion region [9] and in media with quadratic nonlinearity [10], and the self-compression in a weakly relativistic plasma [11, 12]. The methods for pulse shortening based on self-compression are much simpler to implement, because they do not require any additional dispersion elements. At the same time, in contrast to the post-compression methods, the existing methods of self-compression in the visible and near-IR ranges currently have no prospects for energy scaling (this can be done in the mid-IR range due to the existence of materials with anomalous dispersion [9]).

In our previous studies [13–15] we observed for the first time the effect of spectral broadening and self-shortening of negatively chirped pulses in fused silica glass at the second-harmonic wavelength of a Ti:sapphire system (475 nm). Upon interaction with a 1-mm-thick fused silica plate, a 70-fs pulse (previously negatively chirped to 120 fs) was shortened to 26 fs. Then we performed a number of experiments on the interaction of a transform-limited pulse with fused silica in order to determine the shortening mechanisms. Based on the results obtained, we proposed that the pulse shortening is due to the transient regime of multiple filamentation [16]. Under these conditions, multiple filamentation begins to intensively develop in the peak of the radiation pulse, gradually shifting to the pulse leading edge. If the sample is sufficiently thin, filamentation has not enough time to catch the pulse leading edge, in which the radiation retains the initial divergence and forms the central beam core. At the same time, the radiation in the central part and trailing edge of the pulse suffers from strong diffraction and refraction losses in the beam paraxial region. This circumstance allows one to select (using spatial filtering) the radiation from the leading edge with a shorter duration and spectrum red-shifted as a result of the self-phase modulation [16]. Self-shortening of a transform-limited pulse from 87 to 19 fs in a 1-mm-thick fused silica plate was observed in [16]. The formation of a transform-limited pulse at the plate output is due to the fact that the second derivative of the nonlinear phase turns to zero at the leading edge of the initial pulse.

Ya.V. Grudtsyn P.N. Lebedev Physical Institute, Russian Academy of Sciences, Leninsky prosp. 53, 119991 Moscow, Russia; e-mail: jgrudtsin@gmail.com;
A.V. Koribut Moscow Institute of Physics and Technology, Institutskiy per. 9, 141700 Dolgoprudnyi, Moscow region, Russia; P.N. Lebedev Physical Institute, Russian Academy of Sciences, Leninsky prosp. 53, 119991 Moscow, Russia; e-mail: andrew-koribut@yandex.ru;
L.D. Mikheev P.N. Lebedev Physical Institute, Russian Academy of Sciences, Leninsky prosp. 53, 119991 Moscow, Russia; National Research Nuclear University 'MEPhI', Kashirskoe sh. 31, 115409 Moscow, Russia; e-mail: mikheev@sci.lebedev.ru;
V.A. Trofimov M.V. Lomonosov Moscow State University, Vorob'evy gory, 119991 Moscow, Russia; e-mail: vatro@cs.msu.ru

Received 7 March 2018
Kvantovaya Elektronika **48** (4) 306–312 (2018)
Translated by Yu.P. Sin'kov

In this paper, we report the results of studying the evolution of transverse perturbation of the laser beam intensity as the main factor of femtosecond pulse shortening in the transient regime of multiple filamentation in media with Kerr nonlinearity. The analysis was performed using a numerical model developed in cooperation with the Laboratory of Mathematical Modeling in Physics (Moscow State University). The results obtained make it possible to interpret the experimentally found spectral-angular dependences of conical emission.

The pulse shortening regime under study does not require additional dispersive elements to compensate for nonlinear phase and has prospects of energy scaling. Note that this mechanism does not imply an increase in power with a decrease in the pulse duration; therefore, the term 'self-shortening' rather than 'self-compression' is used in our studies.

2. Experimental results and discussion

A schematic of the experiment on interaction of a transform-limited pulse with a thin fused silica plate is shown in Fig. 1a (see [16] for more details).

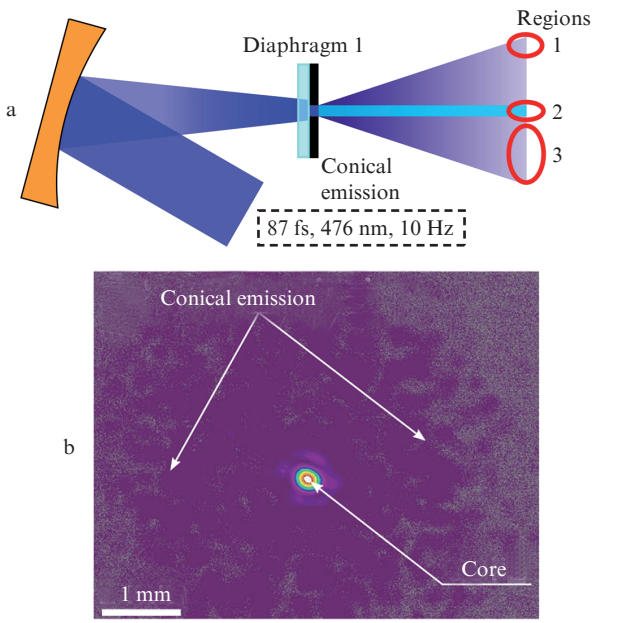

Figure 1. (a) Schematic of the experiment on interaction of a transform-limited pulse with a thin fused silica sample and (b) the radiation profile behind diaphragm 1 at an intensity of 3 TW cm^{-2}.

A convergent femtosecond laser beam (transform-limited 87-fs pulse with a wavelength of 476 nm and energy up to 450 μJ) passed through the sample. A spherical mirror with a focal length of 60 cm was used for focusing; the sample was located at a distance of 7 cm from the waist. The beam diameter in the sample plane was 0.63 mm at a level of $1/e^2$. Diaphragm 1 with a hole diameter of 100 μm was placed directly behind the sample; it transmitted the central part of the beam with a uniformly distributed intensity. The radiation behind diaphragm 1 (Fig. 1b) consisted of a central core (region 2), whose size was independent of the initial beam intensity, and conical emission with a divergence angle increasing with input intensity up to 0.1 rad at 3 TW cm^{-2} (the initial beam convergence angle was less than 0.01 rad). The radiation power transmitted through the diaphragm did not exceed 0.2 GW, and the influence of air nonlinearity in our experiments could be neglected.

The spectral and temporal characteristics of radiation in the beam core (region 2) were investigated in [16]. With an increase in intensity, the main spectral region became red-shifted, the blue-shifted part disappeared, and the pulse duration decreased. At an intensity of 3 TW cm^{-2}, one could observe the formation of a transform-limited 19-fs pulse. We measured the spectra of the core (region 2), the entire conical emission without core (region 3), and the conical emission propagating at an angle of 0.1 rad with respect to the beam axis (region 1).

We also measured separately (using the image transfer method) the radiation profiles at the sample output. The radiation passed through the sample was weakened by two wedges to exclude possible nonlinear effects in air.

The beam profiles recorded at the sample output without diaphragm 1 (Fig. 2) showed that the pulse shortening is accompanied by the development of transverse instability and occurrence of multiple filamentation. According to the Bespalov–Talanov theory [17], the beam is unstable with respect to transverse perturbations with a size $a = (\lambda/n) \times (2n_2I_0)^{-1/2}$, which corresponds to the formation of filaments 7.5 μm in diameter at an intensity of 3 TW cm^{-2}. The diffraction divergence angle $\lambda/a = 6 \times 10^{-2}$ is consistent with the angle of experimentally observed conical emission: ~0.1 rad, a fact indicating to filaments as conical emission sources.

Figure 3 shows experimental emission spectra recorded in the far-field zone (behind diaphragm 1), which exhibit the angular dependence. It can be easily seen that the short-wavelength spectral components propagate at maximum angles. Conical emission with a similar spectral angular dependence is also observed when a single filament is formed in air [18].

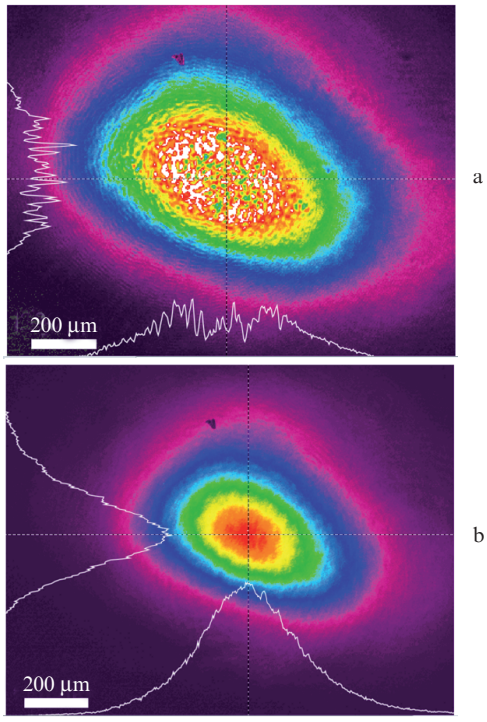

Figure 2. Beam images at the sample output at intensities of (a) 3 and (b) 0.5 TW cm^{-2}.

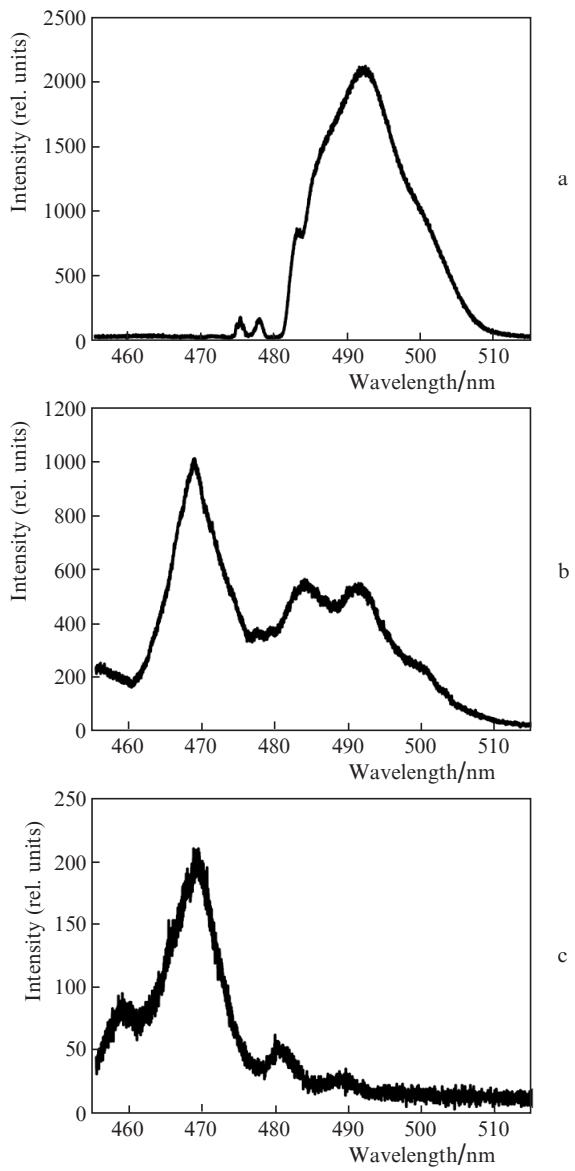

Figure 3. Emission spectra after the transmission through diaphragm 1 at an intensity of 3 TW cm^{-2} for (a) the core (Fig. 1a, region 2), (b) the entire conical emission without core (Fig. 1a, region 3), and (c) the conical emission propagating at an angle of 0.1 rad (Fig. 1a, region 1).

The mechanism of femtosecond pulse self-shortening that was proposed in [16] can additionally be confirmed by carrying out a numerical simulation of the modulational instability under our experimental conditions; this simulation will make it possible to determine the main regularities of the formation of the spectral-angular distribution of radiation behind the sample (in the far-field zone) and compare it with experimental data.

To this end, we numerically simulated the nonlinear propagation of femtosecond radiation, which is characterised by a weak perturbation of intensity on the beam axis, in a Kerr medium. The model is based on solving the nonlinear Schrödinger equation for an axially symmetric case in the slowly varying wave approximation [19], with plasma formation taken into account [20]:

$$\frac{\partial}{\partial\xi}A = \frac{\mathrm{i}\Delta_\perp}{2k_0}A - \frac{\mathrm{i}k^{(2)}}{2}\frac{\partial^2}{\partial\tau^2}A + \frac{\mathrm{i}k_0^2 n_2}{n_0}\Big(1+\frac{\mathrm{i}}{\omega_0}\frac{\partial}{\partial\tau}\Big)\times$$

$$\times\Big[\int_0^\infty R(t')\,|A(\tau-t')|^2dt'\Big]A - \frac{\mathrm{i}k_0}{2n_0^2\rho_\mathrm{c}}\Big(1-\frac{\mathrm{i}}{\omega_0}\frac{\partial}{\partial\tau}\Big)\rho_\mathrm{e}A$$

$$-\frac{1}{2}(\sigma\rho_\mathrm{e}A + \beta_K|A|^{2(K-1)}A),$$

$$\frac{\partial}{\partial\tau}\rho_\mathrm{e} = \frac{\sigma_K}{(\hbar\omega)^K}\rho_\mathrm{nt}|A|^{2K} + \frac{\sigma}{U}\rho_\mathrm{e}|A|^2 - \frac{1}{\tau_\mathrm{r}}\rho_\mathrm{e}.$$

Here, $A(\tau,r,\xi)$ is the complex electric field envelope; $\rho_\mathrm{e}(\tau,r,\xi)$ is the free-charge density; σ_K is the multiphoton absorption cross section; U is the band gap; τ_r is the free-charge recombination time; ρ_nt is the material concentration; σ is the inverse bremsstrahlung absorption cross section; n_2 is the nonlinear refractive index; $k^{(2)}$ is the group-velocity dispersion; β_K is the multiphoton absorption coefficient; ρ_c is the critical plasma density; $R(t) = (1-f_\mathrm{R})\delta(t-t_\mathrm{e}) + f_\mathrm{R}h_\mathrm{R}(t)$; and

$$h_\mathrm{R}(t) = \frac{\tau_1^2+\tau_2^2}{\tau_1\tau_2^2}\exp\Big(-\frac{t}{\tau_2}\Big)\sin\frac{t}{\tau_1}$$

is the function of the molecular part of response with the following parameters for fused silica: $f_\mathrm{R} = 0.18$, $\tau_1 = 12.2$ fs, and $\tau_2 = 32$ fs [21].

The above model takes into account a number of physical processes: diffraction, dispersion, Kerr nonlinearity, self-steepening, stimulated Raman scattering, multiphoton and inverse bremsstrahlung absorption, and the influence of plasma on the refractive index. For simplicity, we modelled the growth of an individual inhomogeneity with a transverse size much smaller than the beam diameter.

With the band gap value of 9 eV [22] and the photon energy of 2.6 eV (at a wavelength of 475 nm), the absorption should be considered as a four-photon process ($K = 4$). According to the Drude model, the inverse bremsstrahlung absorption cross section has the form [23]

$$\sigma = \frac{k_0\omega_0\tau_\mathrm{c}}{n_0\rho_\mathrm{c}(1+\omega_0^2\tau_\mathrm{c}^2)}.$$

Here, τ_c is the collisional time, which characterises the electron–phonon interaction; $\rho_\mathrm{c} = m_\mathrm{e}'\varepsilon_0\omega^2/e^2$; and $m_\mathrm{e}' = 0.86m_\mathrm{e}$ is the electron–hole mass in fused silica [24]. We considered a medium with the following parameters: $n_2 = 3\times10^{-16}$ cm^2 W^{-1} [25], $k^{(2)} = 76$ fs^2 mm^{-1}, $\rho_\mathrm{c} = 4.85\times10^{-21}$ cm^{-3}, $\tau_\mathrm{c} = 23$ fs [26], and $\sigma = 2.6\times10^{-19}$ cm^2.

There is a large spread of the values of the four-photon absorption cross section in the literature [27–30]. Within our model, it was varied in order to obtain best agreement with the experimentally observed spectral-angular dependence of the conical emission intensity and the occurrence threshold of small-scale self-focusing, which was close to 1.5 TW cm^{-2}. Looking ahead, we note that best agreement with experiment was obtained at $\sigma_4 = 7\times10^{-116}$ cm^8 s^3, which is an order of magnitude smaller than the values known from the literature. This choice was made for the following reason: perturbation self-focusing was not obtained in calculations at $\sigma_4 > 10^{-115}$ cm^8 s^3 because of the strong multiphoton absorption and refraction in the plasma formed, which contradicts the observation results.

Calculations were performed for the following conditions: radiation intensity of 3 TW cm^{-2}, beam width of 500 μm, perturbation region diameter of 7.5 μm, and initial perturbation amplitude of 0.2%. It was assumed that the perturbation

source is located on the input sample surface and the phase difference between the fundamental wave and perturbation is zero. Both the beam and perturbation were modelled by a Gaussian, so that the initial amplitude distribution was set by the formula

$$A(r,t) = A_0 \exp\left(-\frac{8r^2}{d_1^2}\right)\left[1 + 0.002\exp\left(-\frac{8r^2}{d_2^2}\right)\right] \times \exp\left(-\frac{2\ln 2t^2}{T_{1/2}^2}\right),$$

where $d_1 = 500$ μm, $d_2 = 7.5$ μm, and $T_{1/2} = 85$ fs.

Numerical simulation showed that the perturbation forms a Kerr lens during beam propagation; this lens leads to spatial localisation of radiation in a microregion behind the unperturbed leading edge of the pulse, with an intensity exceeding the initial one by a factor of 4–5. The results of calculating the field evolution, a comparison of the calculated spectrum of the leading edge with the experimental spectrum of the core, and the results of calculating the electron density as a function of passed distance are presented in Figs 4–7.

The following regions can be selected in the spatiotemporal intensity distribution at the sample output (Fig. 4): a region of strongly divergent trailing edge (selected in Fig. 4a) and a region of radiation focusing and unperturbed leading edge (Fig. 4b). We believe the formation of a core and a shortened pulse in the far-field zone to be related to the existence of the unperturbed leading edge, as confirmed by coincidence of the experimentally obtained core spectrum and numerically calculated spectrum of the pulse leading edge at the sample output (Fig. 5). An additional argument is the decrease in the leading edge duration by a factor of 2–3, which was obtained in calculation (Fig. 4b).

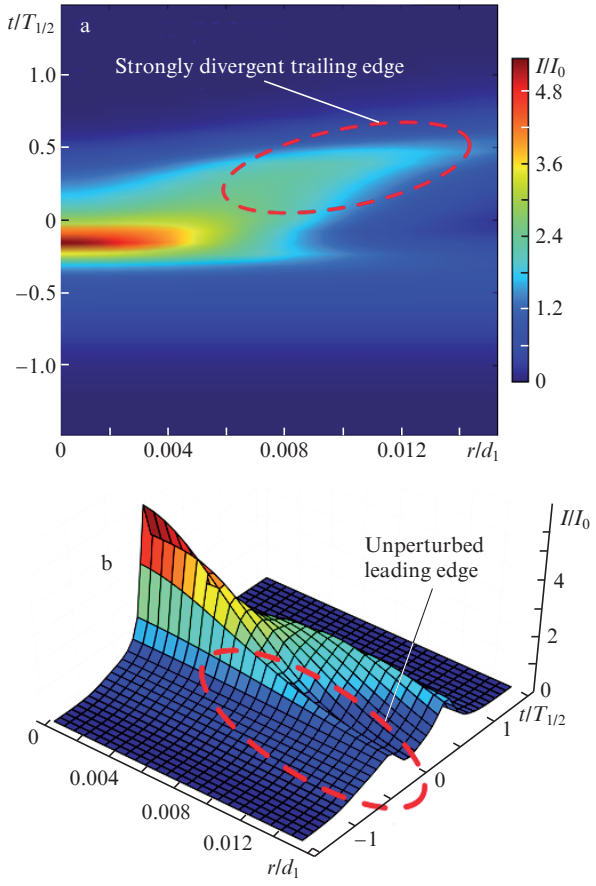

Figure 4. Spatiotemoral intensity distribution within diaphragm 1 at the sample output: (a) top view and (b) view from the side of the leading edge. Here and in Fig. 6, intensities are normalised to the initial maximum beam intensity, time is normalised to the pulse FWHM, and the radius is normalised to the beam diameter at half maximum.

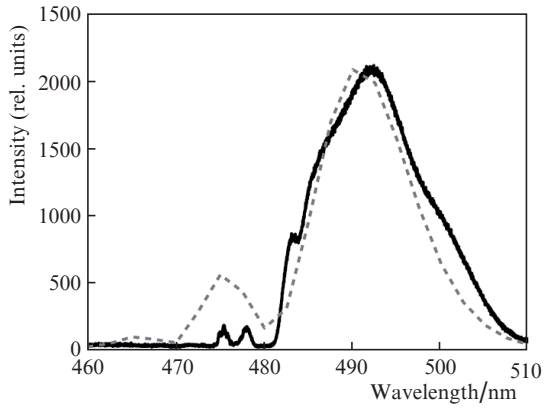

Figure 5. Experimental spectrum of the core (Fig. 1a, region 2) (solid line) and the spectrum for the leading edge at the sample output, obtained by numerical simulation at an intensity of 3 TW cm^{-2} (dashed line).

The development of instability in a sample as a function of the distance passed is demonstrated in Fig. 6. The filament formation begins near the temporal maximum of the pulse, with a small shift to the pulse trailing edge (Figs 6a, 6b), which is caused by the delay of the molecular part of the nonlinear response. Then the intensity becomes approximately constant and exceeds the initial value by a factor of 4–5 (Figs 6c, 6d). The peak intensity shifts towards the leading edge, whereas the radiation from the trailing edge (because of the refraction in the plasma formed) becomes a divergent wave.

Figure 7 illustrates the plasma generation in the filament formed; here, the rate of an increase in the electron density with an increase in radiation intensity can be described by a power-law dependence. As can be seen in Figs 7c and 7d, the electron density stops increasing when the intensity becomes constant (see Figs 6c, 6d). Under these conditions, a plasma channel is formed, where the electron density reaches a value of 2.9×10^{19} cm^{-3} (0.7% of critical). The refraction caused by the plasma of this channel increases additionally the radiation divergence in comparison with the diffraction at the perturbation leading edge. This circumstance explains the experimentally observed (see Fig. 3) larger angle of propagation for the radiation in the short-wavelength wing of the spectrum (which corresponds to the perturbation trailing edge) in comparison with the propagation angle for the long-wavelength wing, which is generated at the perturbation leading edge.

This can easily be shown from the following considerations. The refractive index gradient in the plasma channel is

$$\mathrm{grad}n = \frac{-(2n_0)^{-1}\rho_e/\rho_{ecrit}}{d_2/4},$$

where ρ_{ecrit} is the critical plasma density; d_2 is the filament diameter;

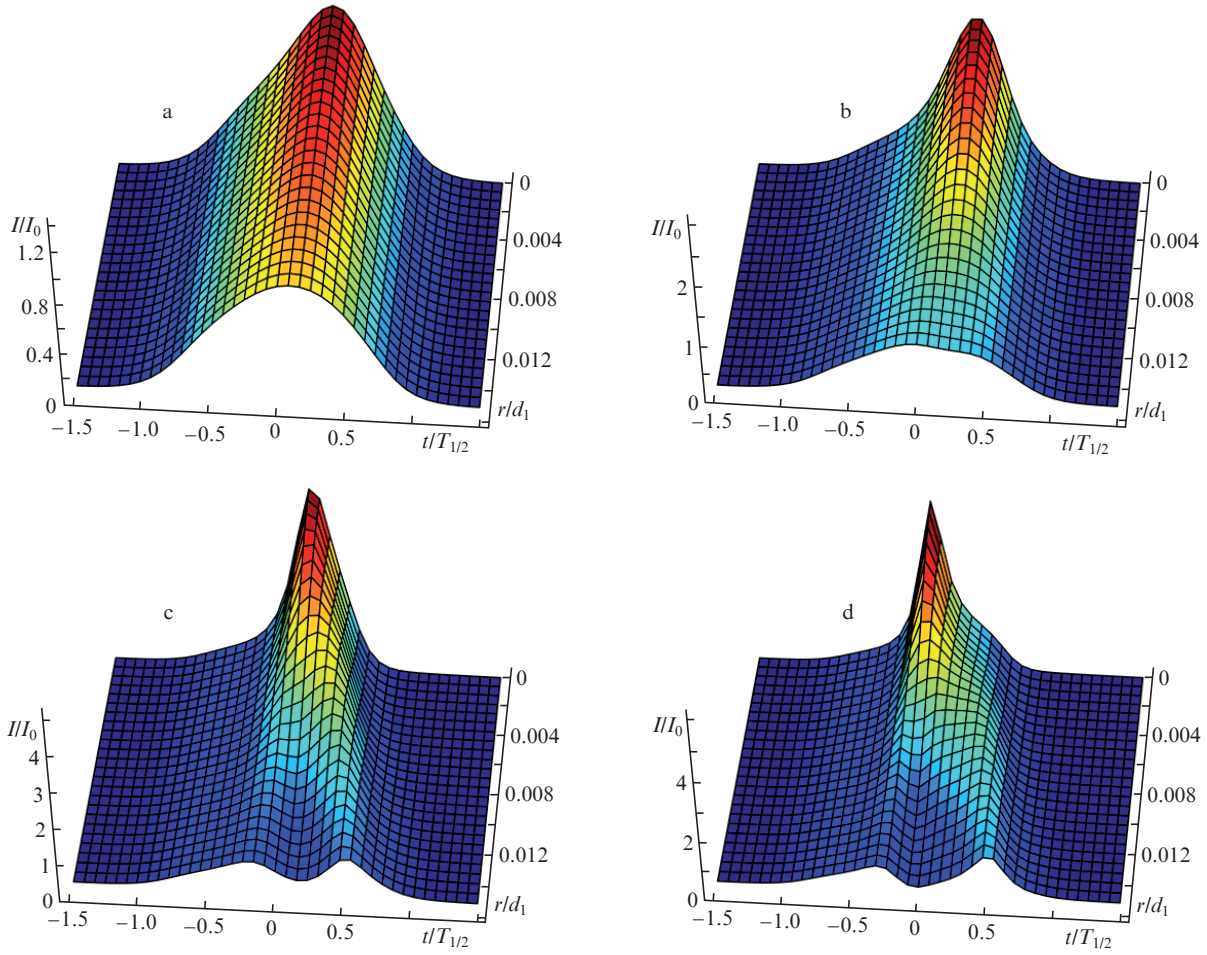

Figure 6. Evolution of perturbation in a sample in dependence of passed distance: (a) 0.7, (b) 0.8, (c) 0.9, and (d) 1.0 mm.

$$n_0 L \operatorname{grad} n = 2\frac{-(\rho_e/\rho_{ecrit})L}{d_2}$$

is the ray deviation angle; and L is the plasma channel length. Having substituted the filament diameter d_2 = 7.5 μm, a plasma channel length of 100 μm, and ρ_e/ρ_{ecrit} = 0.007, we find the total divergence angle to be 0.4. Therefore, the refraction in plasma affects more strongly the divergence than the diffraction $\lambda/d_2 \approx 0.06$. For this reason, the radiation from the perturbation trailing edge, related to the short-wavelength spectral region, diverges much more strongly than the radiation from the leading edge, where the plasma density is low.

Figure 8 shows the calculated spectrum of perturbation in the far-field zone and the experimental spectra of conical emission (see Figs 3b and 3c). To calculate the angular distribution of the perturbation spectrum in the far-field zone, we selected an emitting region with perturbation at the sample output. Then we performed direct calculations of the far-field zone using the Green's function. The calculated spectrum presented in Fig. 8a is the result of integration over propagation angles from 0.02 to 0.1 rad, a range corresponding to the experimentally observed spectrum of the entire conical emission. Figure 8b shows the spectra obtained by calculation and experimentally for the conical emission propagating, respectively, at angles of 0.085 and 0.1 rad with respect to the beam axis.

Agreement between the calculated and experimental results, which is indicative of the general dominance of the short-wavelength wing in the spectrum at the conical emission periphery (at an angle of 0.1 rad), confirms our suggestion about the origin of the experimentally observed angular dependence of the conical emission spectrum and the important role of plasma in the formation of this dependence.

3. Conclusions

Using numerical simulation of the nonlinear interaction of 476-nm femtosecond radiation with a 1-mm-thick fused silica sample, we justified the proposed mechanism of self-shortening of femtosecond pulses in the visible range that propagate in Kerr media (the mechanism is based on the transient regime of multiple filamentation formation). The rise of the transverse spatial instability, which plays a determining role in the formation of multiple filamentation, is demonstrated by an example of a single perturbation of the wave amplitude. The calculated spectral angular dependences turned out to be in good agreement with experimental data, a fact confirming the adequacy of the proposed theoretical model.

The numerical simulation showed also that the experimentally observed multiple filamentation in a thin fused silica sample may occur only at four-photon absorption cross sections no larger than 10^{-115} cm^8 s^3. This value is smaller by more than an order of magnitude than the generally accepted ones (obtained for KBr, KI, NaCl, TeO_2, and GeS_2), which lie in the range from $2 \times 10^{-112} - 10^{-114}$ cm^8 s^3 [27–30].

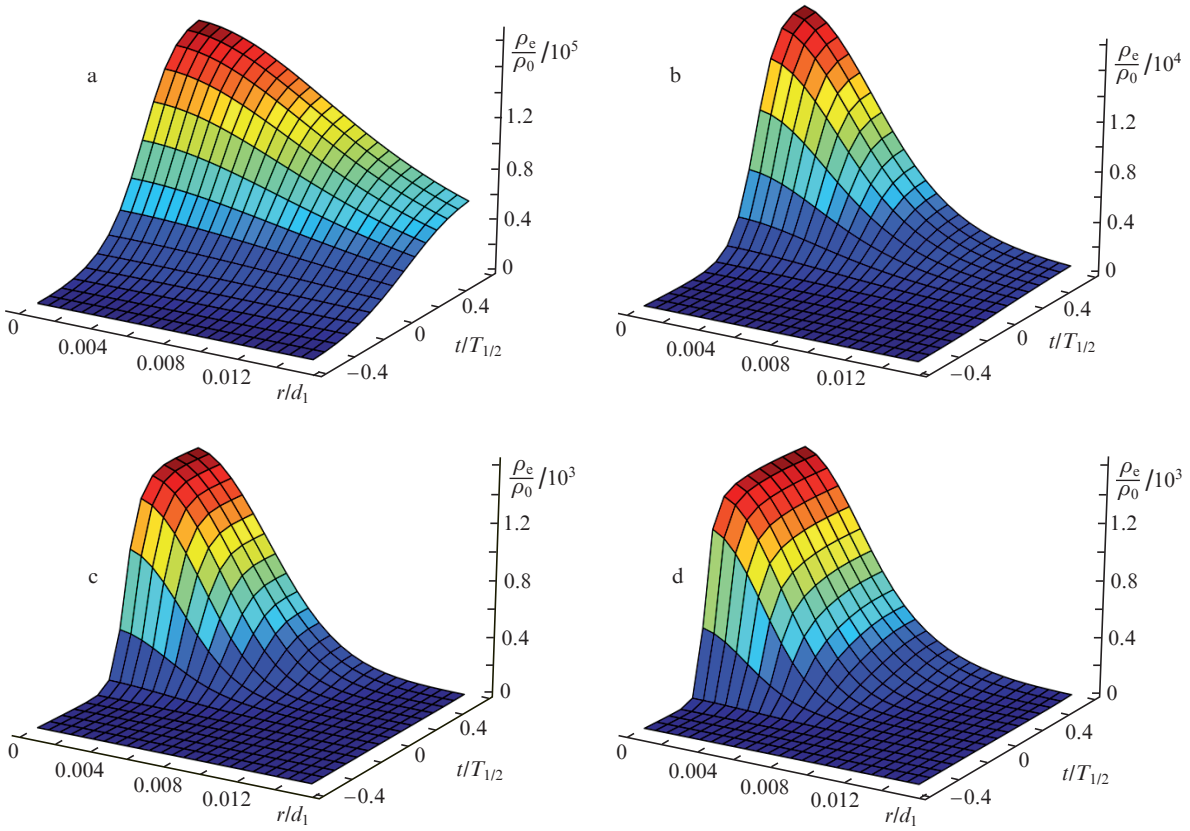

Figure 7. Evolution of the spatiotemporal profile of electron density in a sample in dependence of passed distance: (a) 0.7, (b) 0.8, (c) 0.9, and (d) 1.0 mm. The densities are normalised to the material density $\rho_0 = 2.1 \times 10^{22}$ cm^{-3}, the time is normalised to the pulse FWHM, and the radius is normalised to the beam diameter at half maximum.

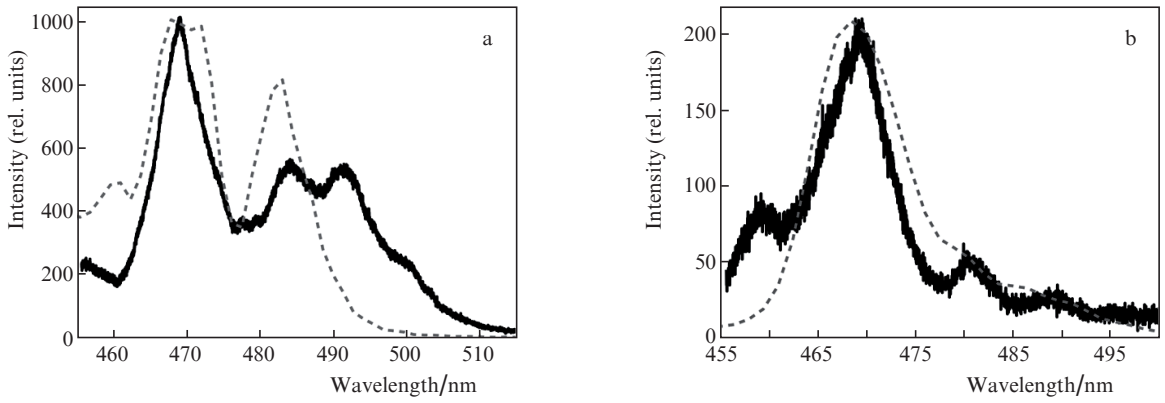

Figure 8. (a) Experimental spectrum of the entire conical emission without core (solid line) and a calculated spectrum of perturbation, integrated over angle in the range from 0.02 to 0.1 rad (dashed line), and (b) the conical emission spectrum measured at an angle of 0.1 rad with respect to the beam axis (solid line) and the calculated spectrum of perturbation for the radiation propagating at an angle of 0.085 rad with respect to the beam axis (dashed line).

Acknowledgements. This work was supported by the Presidium of the Russian Academy of Sciences (Programme 'Extreme Light Fields and Their Interaction with Matter') and the Competitiveness Growth Programme of the National Research Nuclear University 'MEPhI'.

References

1. Kobayashi T., Shirakawa A., Fuji T. *IEEE J. Sel. Top. Quantum Electron*., **7**, 525 (2001).
2. Gildenburg V.B., Vvedenskii N.V. *Phys. Rev. Lett*., **98**, 245002 (2007).
3. Kim A.V., Ryabkin M.Yu., Sergeev A.M. *Usp. Fiz. Nauk*, **169**, 58 (1999).
4. Rolland C., Corkum P.B. *J. Opt. Soc. Am. B*, **5**, 641 (1988).
5. Mourou G., Mironov S., Khazanov E., Sergeev A. *Eur. Phys. J. Spec. Top*., **223**, 1181 (2014).
6. Stibenz G., Zhavoronkov N., Steinmeyer G. *Opt. Lett*., **31**, 274 (2006).
7. Zair A., Guandalini A., Schapper F., Holler M., Biegert J., Gallmann L., Keller U. *Opt. Express*, **15**, 5394 (2007).
8. Kurilova M.V., Uryupina D.S., Mazhorova A.V., Volkov R.V., Gorgutsa S.R., Panov N.A., Kosareva O.G., Savel'ev A.B.

Quantum Electron., **39**, 879 (2009) [*Kvantovaya Elektron*., **39**, 879 (2009)].
9. Shumakova V., Malevich P., Ališauskas S., Voronin A., Zheltikov A.M., Faccio D., Kartashov D., Baltuška A., Pugžlys A. *Nature Commun*., **7**, 12877 (2016).
10. Ashihara S., Nishina J., Shimura T., Kuroda K. *J. Opt. Soc. Am. B*, **19**, 2505 (2002).
11. Faure J., Glinec Y., Santos J.J., Ewald F., Rousseau J.P., Kiselev S., Hosokai T., Malka V. *Phys. Rev. Lett*., **95**, 205003 (2005).
12. He Z.-H., Nees J.A., Hou B., Krushelnick K., Thomas A.G.R. *Phys. Rev. Lett*., **113**, 263904 (2014).
13. Aristov A.I., Grudtsyn Ya.V., Mikheev L.D., Polivin A.V., Stepanov S.G., Trofimov A.V., Yalovoi V.I. *Quantum Electron*., **42**, 1097 (2012) [*Kvantovaya Elektron*., **42**, 1097 (2012)].
14. Alekseev S.V., Aristov A.I., Grudtsyn Ya.V., Ivanov N.G., Koval'chuk B.M., Losev V.F., Mamaev S.B., et al. *Quantum Electron*., **43**, 190 (2013) [*Kvantovaya Elektron*., **43**, 190 (2013)].
15. Grudtsyn Ya.V., Zubarev I.G., Koribut A.V., Kuchik I.E., Mamaev S.B., Mikheev L.D., Semenov S.L., Stepanov S.G., Trofimov V.A., Yalovoi V.I. *Quantum Electron*., **45**, 415 (2015) [*Kvantovaya Elektron*., **45**, 415 (2015)].
16. Grudtsyn Ya.V., Koribut A.V., Trofimov V.A., Mikheev L.D. *J. Opt. Soc. Am. B*, **35**, 1054 (2018).
17. Bespalov V.I., Talanov V.I. *Pis'ma Zh. Eksp. Teor. Fiz*., **3**, 471 (1966).
18. Nibbering E.T.J., Curley P.F., Grillon G., Prade B.S., Franco M.A., Salin F., Mysyrowicz A. *Opt. Lett*., **21**, 62 (1996).
19. Brabec T., Krausz F. *Phys. Rev. Lett*., **78**, 3282 (1997).
20. Skupin S., Bergé L. *Phys. D: Nonl. Phenomena*, **220**, 14 (2006).
21. Blow K.J., Wood D. *IEEE J. Quantum Electron*., **25**, 2665 (1989).
22. Arnold D., Cartier E., DiMaria D.J. *Phys. Rev. B*, **45**, 1477 (1992).
23. Stuart B.C., Feit M.D., Herman S., Rubenchik A.M., Shore B.W., Perry M.D. *Phys. Rev. B*, **53**, 1749 (1996).
24. Zafar S., Conrad K.A., Liu Q., Irene E.A., Hames G., Kuehn R., Wortman J.J. *Appl. Phys. Lett*., **67**, 1031 (1995).
25. Stolen R.H., Ashkin A. *Appl. Phys. Lett*., **22**, 294 (1973).
26. Sudrie L., Couairon A., Franco M., Lamouroux B., Prade B., Tzortzakis S., Mysyrowicz A. *Phys. Rev. Lett*., **89**, 186601 (2002).
27. Catalano I.M., Cingolani A., Minafra A. *Phys. Rev. B*, **5**, 1629 (1972).
28. Jones S.C., Fischer A.H., Braunlich P., Kelly P. *Phys. Rev. B*, **37**, 755 (1988).
29. Shen X.A., Jones S.C., Braunlich P., Kelly P. *Phys. Rev. B*, **36**, 2831 (1987).
30. Bindra K.S., Bookey H.T., Kar A.K., Wherrett B.S., Liu X., Jha A. *Appl. Phys. Lett*., **79**, 1939 (2001).